Knowledge-Based Systems 342 (2026) 115912

Contents lists available at ScienceDirect

Knowledge-Based Systems

journal homepage: www.elsevier.com/locate/knosys

Neural network-based systematics of giant dipole resonance parameters and impact on (γ,n) reaction cross sections

Murat Dag

Vocational School of Health Services, Kirsehir Ahi Evran University, Kirsehir 40100, Turkiye

ARTICLE INFO

Keywords:
Giant Dipole Resonance (GDR)
(γ,n) Reaction cross sections
Artificial neural networks
Nucleus-wise validation
TALYS 2.0

ABSTRACT

Reliable giant dipole resonance (GDR) parameterization is essential for photonuclear reaction modeling in the (γ, n) reaction energy region, where dipole absorption dominates. This work develops a staged artificial neural network (ANN) scheme to infer the GDR centroid energy, width, and peak cross section from physically motivated nuclide descriptors compiled from evaluated nuclear-structure information provided by the National Nuclear Data Center (NNDC), using Reference Input Parameter Library (RIPL-3) values as learning targets. To obtain performance estimates that reflect genuine transfer to unseen nuclei and to avoid leakage from repeated entries, the dataset was partitioned nucleus-wise, assigning all records of a given nuclide to a single subset. Parameter inference was organized in three sequential stages to preserve the established coupling among centroid energy, width, and peak strength. A SHAP-based interpretability analysis was performed at each stage to quantify the relative importance of the input descriptors. The resulting ANN-derived parameter sets were implemented in TALYS and compared with the nucleus-specific GDR parameters internally available in the built-in TALYS structure/gamma/gdr/ data files under otherwise identical reaction-model conditions. Their impact on calculated (γ,n) reaction excitation functions was evaluated against experimental photoneutron reaction cross sections from the EXFOR library via the JANIS interface, quantifying agreement with experiment achieved by the neural-network-based GDR systematics. The even-even 112–124Sn isotopic chain was examined as a representative case of isotopic continuity. Overall, implementation of the ANN-derived GDR parameter triplets in TALYS generally improves agreement between calculated (γ,n) reaction excitation functions and EXFOR data relative to the built-in nucleus-specific TALYS GDR values where available.

1. Introduction

Photonuclear reactions provide a well-established probe of nuclear response under electromagnetic excitation and supply essential input for radiation transport calculations, shielding design, activation studies, safeguards-related analyses, and neutron-source development. For photon energies below roughly 30 MeV, which covers most practical (γ, n) reaction applications, the total photoabsorption cross section in medium-mass and heavy nuclei is governed predominantly by Giant Dipole Resonance (GDR). In this regime, the dipole response is characterized by a collective isovector mode that concentrates a substantial fraction of the E1 strength into a broad resonance structure [1–2].

The GDR is conventionally interpreted as an out-of-phase oscillation of protons against neutrons. Its characteristic mass dependence was captured by early macroscopic descriptions such as the Goldhaber–-Teller and Steinwedel–Jensen models [3–4], while later microscopic particle–hole approaches—within shell-model and random-phase-approximation formalisms—clarified the collective origin of the response and the mechanisms responsible for damping and fragmentation of the strength, particularly in medium-mass and heavy systems [5–6].

Systematic experimental surveys based on bremsstrahlung, quasi-monoenergetic annihilation photons, and tagged-photon measurements have established regular trends in centroid energy, width, and integrated strength across the nuclide chart. These analyses confirm that the GDR exhausts a substantial fraction of the Thomas–Reiche–Kuhn [7–8] dipole sum rule and exhibits a clear mass dependence: centroid energies decrease with increasing mass number, taking values near 20–25 MeV in light nuclei and approximately 13–15 MeV in heavy systems [9]. In deformed nuclei, the resonance may split into two components associated with oscillations along distinct principal axes; the magnitude of this splitting correlates with the quadrupole deformation parameter β_2. Global evaluations further demonstrate systematic mass number-dependent trends in centroid energy and spreading width along

E-mail address: muratdag@ahievran.edu.tr.

https://doi.org/10.1016/j.knosys.2026.115912
Received 24 February 2026; Received in revised form 21 March 2026; Accepted 31 March 2026
Available online 1 April 2026

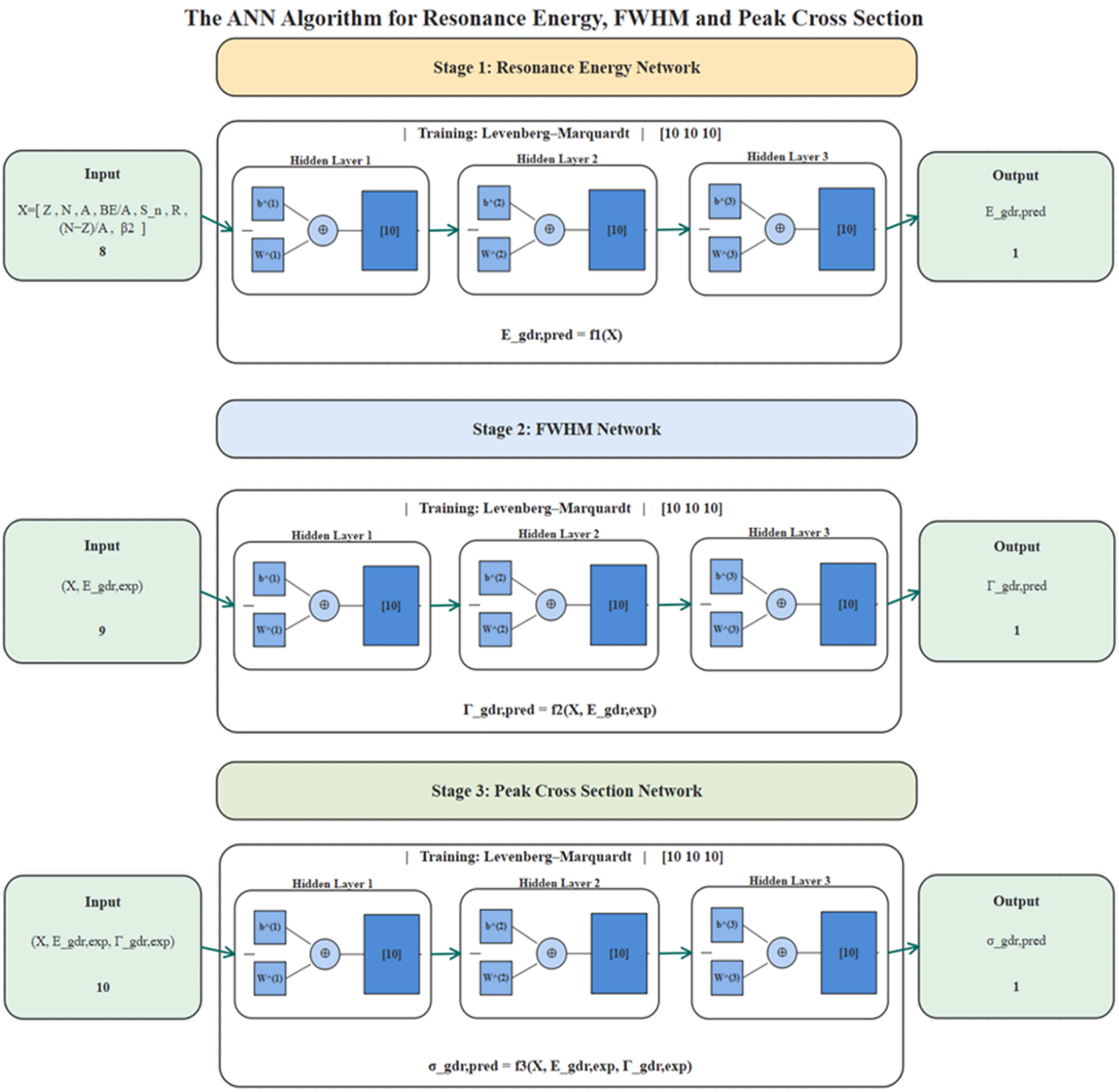

Fig. 1. Staged ANN framework used to estimate the GDR parameters.

isotopic chains [10–12].

Within the phenomenological representation commonly used in reaction calculations, the total photonuclear reaction cross section is expressed as the sum of dipole, quasi-deuteron, and photon–meson contributions [13–14],

$$\sigma_T(E_\gamma) = \sigma_{\mathrm{gdr}}(E_\gamma) + \sigma_{\mathrm{qd}}(E_\gamma) + \sigma_{\mathrm{pm}}(E_\gamma) \tag{1}$$

with the dipole term providing the dominant contribution in the energy interval that most strongly influences (γ,n) reactions in medium-mass and heavy nuclei . In Lorentzian form, the dipole term is parameterized as

$$\sigma_{\mathrm{gdr}}(E_\gamma) = \sigma_{\mathrm{gdr}} \frac{E_\gamma^2 \Gamma_{\mathrm{gdr}}^2}{\left(E_\gamma^2 - E_{\mathrm{gdr}}^2\right)^2 + E_\gamma^2 \Gamma_{\mathrm{gdr}}^2} \tag{2}$$

where E_γ, E_{gdr}, Γ_{gdr} and σ_{gdr} denote the photon energy, the centroid energy of resonance, full width at half maximum (FWHM), and peak cross section, respectively. Collectively, these quantities define the centroid energy of the resonance, its damping width reflecting spreading mechanisms, and the peak magnitude of the dominant E1 absorption component implemented in reaction modeling.

Empirical systematics [15] are frequently used to provide baseline parameter estimates. The centroid energy E_{gdr} is expressed as

$$E_{\mathrm{gdr}} = 31.2A^{-1/3} + 20.6A^{-1/6} \tag{3}$$

while the width is correlated with the centroid via

$$\Gamma_{\mathrm{gdr}} = 0.026E_{\mathrm{gdr}}^{1.91} \tag{4}$$

Although approximate, such relationships capture the observed interdependence of centroid energy and width across broad regions of the nuclide chart and remain widely used in practical implementations.

In reaction calculations, photon-strength parameters are commonly adopted from evaluated libraries such as the Reference Input Parameter Library (RIPL-3) [16]; in the present work, the experimentally evaluated

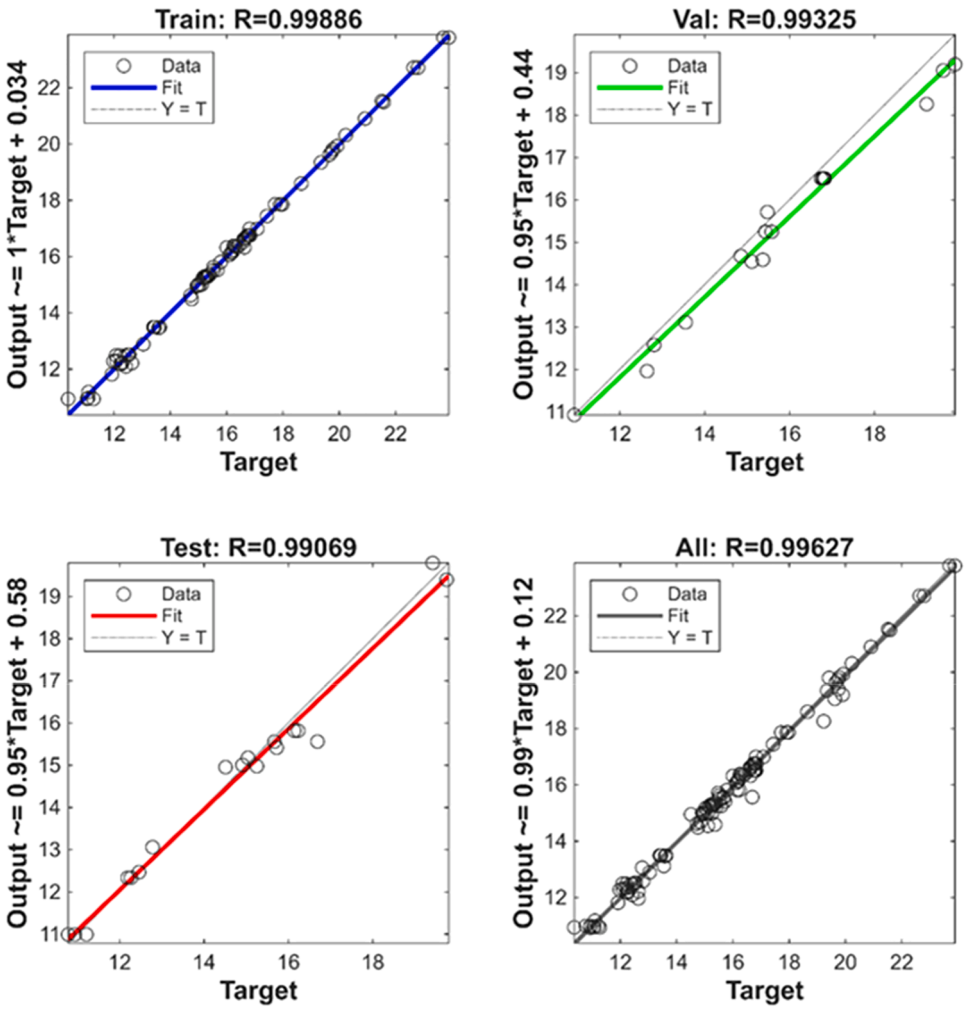

Fig. 2. Regression plots for the Stage 1 ANN model predicting E_{gdr}. In all panels, the horizontal axis represents the target E_{gdr} values and the vertical axis repsresents the ANN-predicted E_{gdr} values; both axes are given in MeV. Results are shown separately for the training, validation, test, and combined datasets under nucleus-wise partitioning.

GDR parameters provided in Experimental Giant Dipole Resonance (GDR) Parameters in RIPL-3 are used specifically as supervised learning targets for ANN training rather than as direct reaction-model inputs. While indispensable, evaluated datasets can exhibit uneven isotopic coverage and may reflect heterogeneity stemming from different experimental inputs, analysis choices, and evaluation protocols. When explicit parameter information is missing for a given nuclide, reaction codes typically revert to internal defaults or simplified prescriptions; such fallbacks can disrupt isotopic continuity and, for specific nuclei, contribute to discrepancies between calculated photoneutron reaction excitation functions and measured data.

Motivated by these limitations, machine-learning approaches [17–21] have recently been explored as tools to estimate GDR parameters across nuclei. The present study combines evaluated nuclear-structure data, evaluated GDR parameter systematics, machine-learning inference, and reaction-model validation within a single consistent workflow. Multitask neural networks have been employed for the joint estimation of GDR centroid energies and widths, and staged estimation schemes have combined physically motivated descriptors with explicit evaluation of their impact by propagating the inferred parameters into reaction-code calculations. These studies collectively indicate that data-driven parameter inference can be integrated into established photonuclear reaction modeling practice.

Although the present study is centered on ANN-based inference of GDR parameters rather than on direct regression of reaction cross sections, it is important to note that machine-learning approaches have also increasingly been applied to nuclear reaction cross-section modeling itself, including photonuclear and neutron-induced reactions. This broader line of work provides an important context for the present study, since the ANN-inferred GDR parameters are ultimately evaluated here through their impact on calculated $(\gamma,)$ reaction excitation functions. In contrast to direct cross-section prediction studies, however, the objective of the present work is to improve a physically meaningful intermediate parameterization layer, namely the GDR centroid energy, width, and peak cross section, and to test its propagation within TALYS under fixed reaction-model conditions.

A central methodological issue in this context is data partitioning. Compiled photonuclear reaction datasets commonly include multiple entries per nuclide, originating from distinct experiments, normalization choices, or restricted energy ranges. If the data are split row-wise, records from the same nuclide can appear in both training and evaluation subsets, creating information leakage and artificially inflating apparent predictive performance. Moreover, when multiple entries exist for a given nuclide, selecting only a single representative record (e.g., one evaluation or one experimental dataset) can introduce a selection dependence and potentially shift the learned mapping, because the target values may vary across entries due to systematic and normalization differences. This is most critical for isotopic-chain systematics, because the meaningful test is whether the model extrapolates to new nuclides, not whether it reproduces repeated measurements of a nuclide

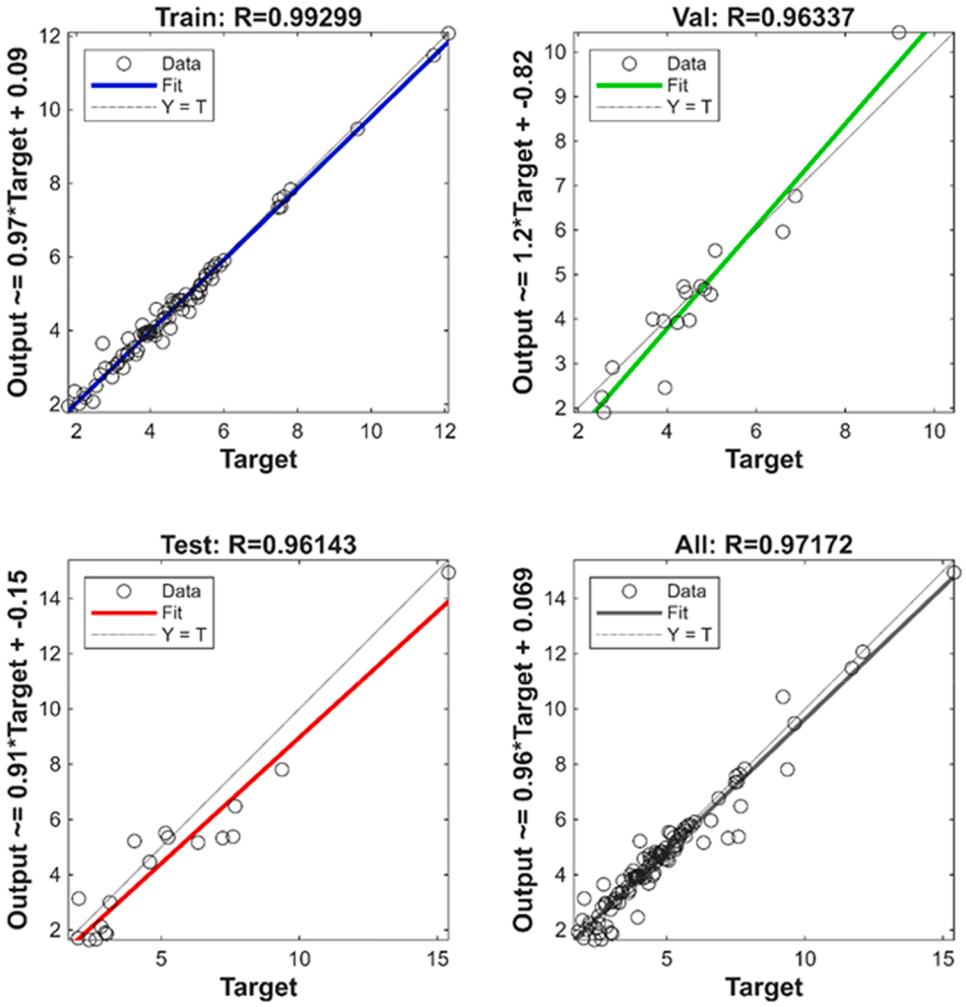

Fig. 3. Regression plots for the Stage 2 ANN model predicting Γ_{gdr}. In all panels, the horizontal axis represents the target Γ_{gdr} values and the vertical axis represents the ANN-predicted Γ_{gdr} values; both axes are given in MeV. Results are shown separately for the training, validation, test, and combined datasets under nucleus-wise partitioning.

already seen in training.

The present study addresses this point explicitly by adopting a nucleus-wise holdout strategy in which all records associated with a given nuclide are assigned to a single subset. On this basis, a three-stage ANN framework is constructed to infer E_{gdr}, Γ_{gdr}, and σ_{gdr} from eight physically motivated nuclear descriptors. The predicted parameter triplets $(E_{gdr,pred}, \Gamma_{gdr,pred}, \text{and } \sigma_{gdr,pred})$ are then implemented in the TALYS 2.0 code [22] for nuclear reaction calculations by overriding the default strength parameterization; and the resulting (γ,n) reaction excitation functions are evaluated against experimental data and against calculations performed using the code's default settings. A case study is carried out along the even–even tin isotopic chain ($^{112–124}$Sn), enabling a systematic assessment of isotopic continuity and of the reaction-level implications of the learned parameter systematics. The even–even $^{112–124}$Sn chain was selected as a controlled isotopic case study because it provides a contiguous and structurally coherent sequence with suitable experimental photoneutron reaction data for reaction-level validation; in addition, it includes nuclei both with and without built-in TALYS GDR entries, allowing the practical impact of the ANN-based parameterization to be assessed under both complete and incomplete default-library conditions.

In this respect, the distinct contribution of the present study lies not in the use of ANN alone, but in the combination of leakage-controlled nucleus-wise validation, staged inference of the coupled GDR parameter triplet, stage-wise SHAP-based interpretability, and direct reaction-level testing through TALYS under fixed modeling conditions. Relative to earlier ML-based GDR studies, the framework is designed specifically to evaluate transferable nuclide-level inference while preserving isotopic continuity and examining how the inferred parameter systematics propagate to calculated (γ, n) reaction excitation functions.

Accordingly, the objectives are: (i) to construct a staged ANN-based estimator of GDR centroid energy, width, and peak cross section from physically motivated nuclide descriptors; (ii) to quantify predictive performance under nucleus-wise validation; (iii) to examine the relative importance of the input quantities through stage-wise SHAP analysis; and (iv) to evaluate the impact of the inferred parameters on calculated photoneutron reaction excitation functions within a fixed reaction-modeling environment.

2. Methods

Artificial neural networks are employed as nonlinear regression operators to map nuclide-level descriptors onto the three parameters defining the Lorentzian representation of the GDR. The framework used here is explicitly staged in order to preserve the hierarchical coupling among the parameters while enforcing strict nucleus-wise separation between training and evaluation. The subscripts "exp" and "pred" denote, respectively, target values taken from the compiled dataset and the corresponding ANN outputs.

Each nucleus is represented by an eight-component descriptor vec-

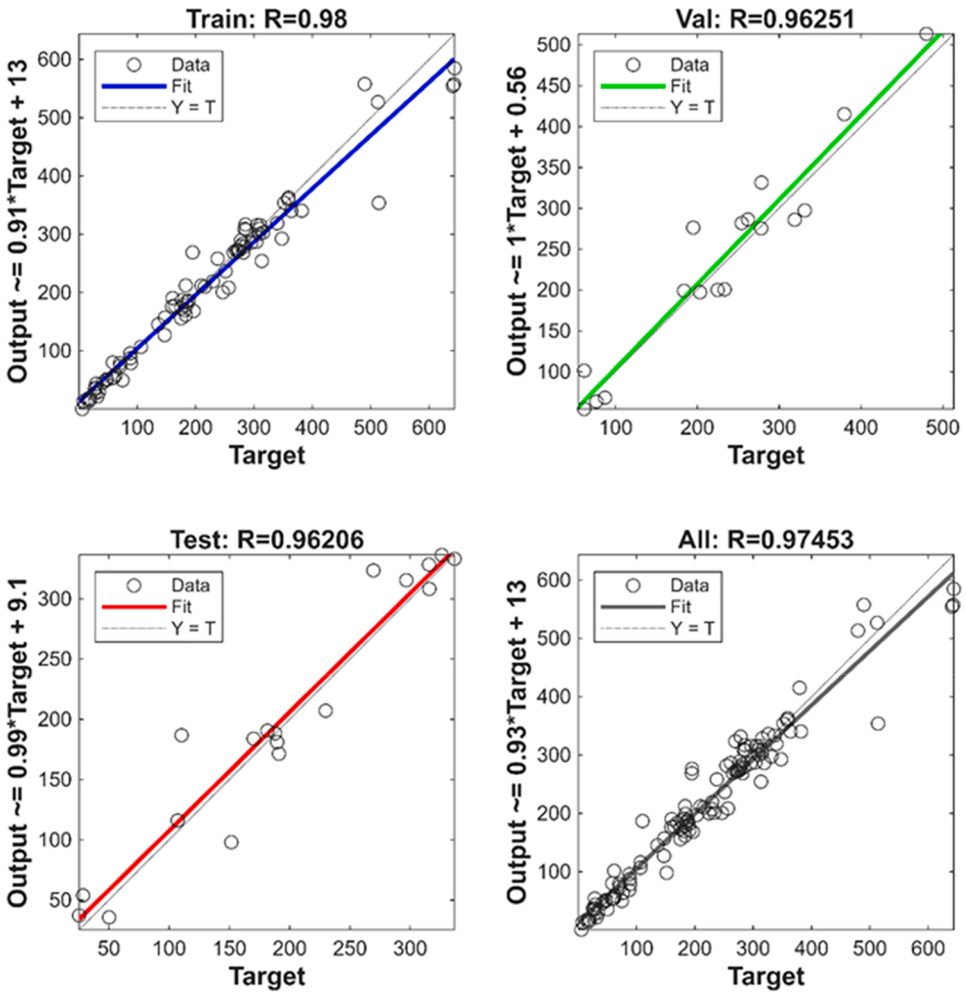

Fig. 4. Regression plots for the Stage 3 ANN model predicting σ_{gdr}. In all panels, the horizontal axis represents the target σ_{gdr} values and the vertical axis represents the ANN-predicted σ_{gdr} values; both axes are given in mb. Results are shown separately for the training, validation, test, and combined datasets under nucleus-wise partitioning.

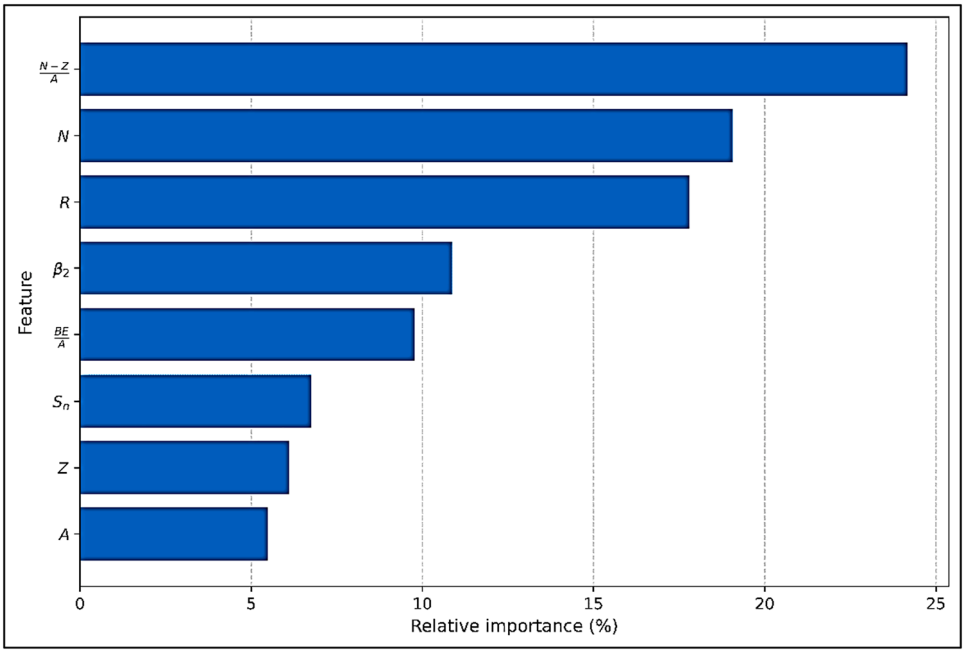

Fig. 5. SHAP-based relative feature importance for Stage 1, corresponding to the ANN-based inference of E_{gdr} from the eight base nuclide descriptors.

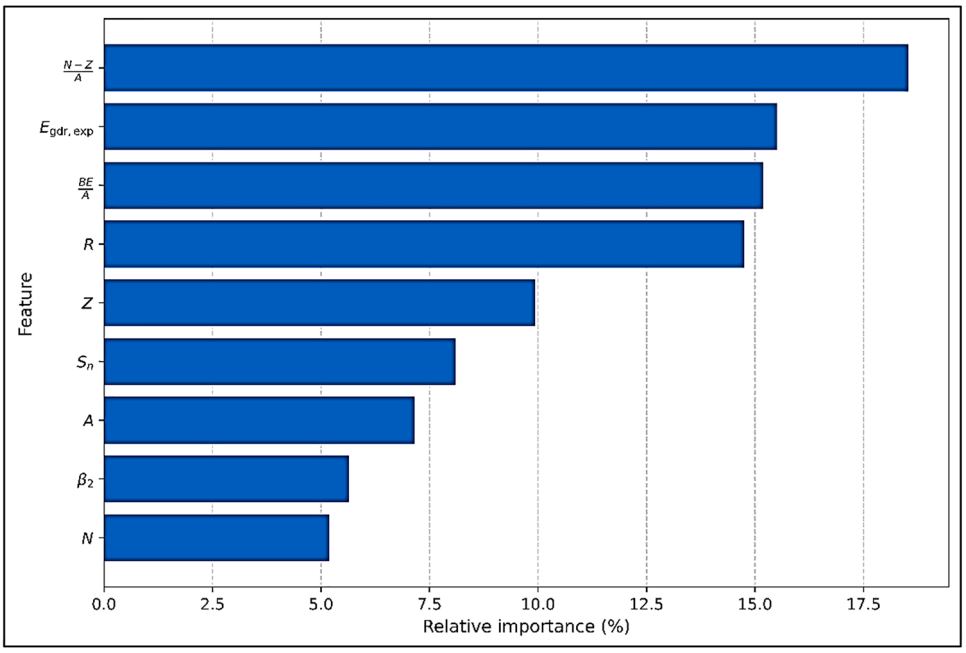

Fig. 6. SHAP-based relative feature importance for Stage 2, corresponding to the ANN-based inference of Γ_{gdr} from the augmented input set.

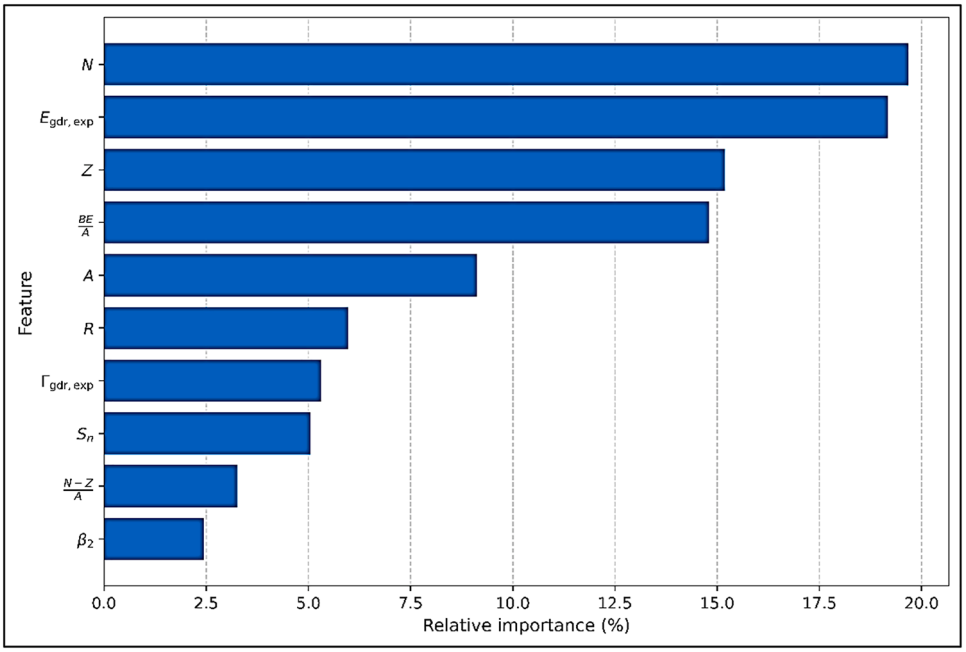

Fig. 7. SHAP-based relative feature importance for Stage 3, corresponding to the ANN-based inference of σgdr from the augmented input set.

tor, as seen in Eq. (5), combining composition variables, binding-related quantities, geometric scaling, isospin asymmetry, and quadrupole deformation,

$$\mathrm{X} = \left[Z, N, A, \frac{BE}{A}, S_n, R, \frac{N-Z}{A}, \beta_2\right], R = 1.2A^{1/3}. \quad (5)$$

In the present framework, spherical and deformed nuclei are not separated a priori into distinct classes. Instead, deformation information is incorporated directly into the common descriptor vector through the quadrupole deformation parameter β_2, so that both types of nuclei are retained within the same learning framework. Accordingly, deformation effects are treated at the descriptor level within the adopted single-component Lorentzian GDR representation, rather than through an explicit class-wise or multi-component treatment of deformation-induced resonance splitting. The nuclear identifiers and associated structural quantities entering the descriptor vector were compiled from evaluated datasets available through the NNDC [23] nuclear data resources, ensuring consistency between nuclear-property inputs and evaluated photonuclear reaction information. The learning targets were the evaluated parameter triplet,

$$\left(E_{gdr,exp}, \Gamma_{gdr,exp}, \sigma_{gdr,exp}\right) \quad (6)$$

These quantities correspond to experimentally evaluated Giant Dipole Resonance parameters compiled in the RIPL-3 library, which

Table 1
GDR centroid energy (E_{gdr}), width (Γ_{gdr}), and peak cross section (σ_{gdr}) for the even–even tin isotopes ($^{112-124}$Sn), together with goodness of fit indicators $(\text{Red.}\chi^2,\ R^2,\ \text{pearson}\,r)$ for calculated (γ,n) reaction cross sections. TALYS calculations were performed using the Brink–Axel Lorentzian option for the GDR strength function (strength function type 2) in both the default and neural-network-based cases, allowing direct modification of GDR parameters through the input file. The default TALYS GDR parameters correspond to the built-in entries provided in the TALYS 2.0 GDR data file (structure/gamma/gdr/sn.gdr). For ^{112}Sn, ^{114}Sn, and ^{122}Sn, no corresponding built-in GDR parameter entry is available; therefore, only neural-network-based parameter sets are reported.

	TALYS 2.0 Built-in GDR Parameters						Neural-Network-Based GDR Parameters					
	$E(MeV)$	$\Gamma\,(MeV)$	$\sigma\,(mb)$	Goodness of Fit Indicators for (γ,n) Reaction Cross Sections (Comparison with Exp Data)			E (MeV)	Γ (MeV)	σ (mb)	Goodness of Fit Indicators for (γ,n) Reaction Cross Sections (Comparison with Exp Data)		
				Red. χ^2	R^2	Pearson r				Red. χ^2	R^2	Pearson r
112Sn	-	-	-	-	-	-	16.07	4.37	233.37	5.922	0.893	0.962
114Sn	-	-	-	-	-	-	15.80	4.20	257.03	7.373	0.957	0.980
116Sn	15.56	5.08	271.00	61.034	0.988	0.997	15.53	4.49	258.95	19.695	0.995	0.998
118Sn	15.44	4.86	279.00	81.169	0.981	0.998	15.25	4.58	268.53	41.102	0.992	0.997
120Sn	15.37	5.10	285.00	44.362	0.993	0.997	15.34	4.79	274.08	32.306	0.996	0.998
122Sn	-	-	-	-	-	-	15.52	4.93	275.57	18.372	0.988	0.996
124Sn	15.28	4.80	276.00	41.518	0.985	0.994	15.30	4.84	275.33	42.066	0.983	0.995

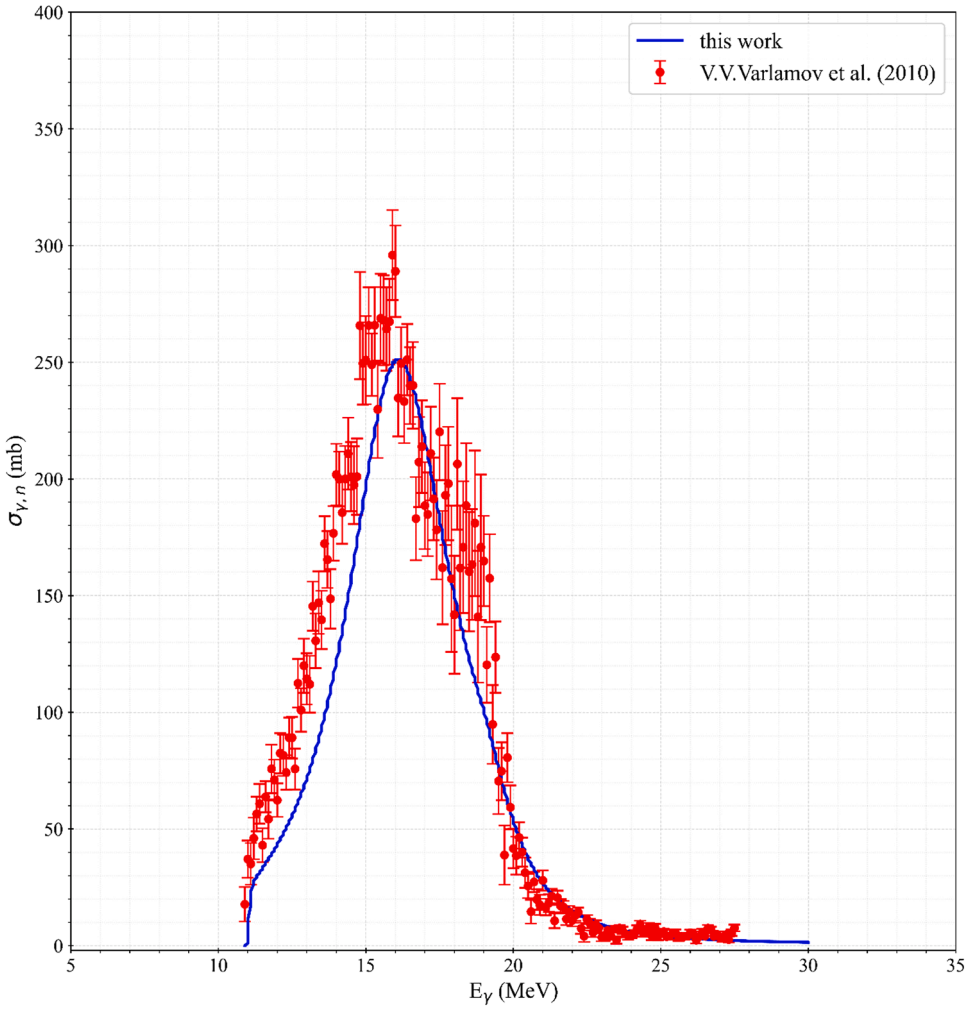

Fig. 8. Calculated (γ, n) reaction cross section for ^{112}Sn obtained within TALYS using neural-network-based GDR parameter systematics.

aggregates experimental photoabsorption analyses into recommended centroid energies, FWHM widths, and peak cross sections. Rather than training a single multi-output regressor, a three-stage estimation scheme was adopted that keeps the coupling among the GDR parameters explicit while retaining the full descriptor information at each step. The eight-component nuclide descriptor vector X served as the common input at all stages, and parameters inferred in earlier stages were appended only to condition subsequent predictions in a manner consistent with established GDR systematics. In Stage 1, the centroid energy E_{gdr}, which fixes the resonance location, is inferred from X. In Stage 2, the width Γ_{gdr} is learned from the augmented input $(X_{,gdr})$, reflecting the empirically observed interdependence between centroid energy and spreading width. In Stage 3, the Lorentzian peak cross section *σgdr* is inferred from $(X_{,\text{gdr}},\ \Gamma_{\text{gdr}})$, acknowledging that the peak normalization is not independent of the resonance energy scale and damping. The three stages are defined as seen in Eqs. (7), (8) and (9).

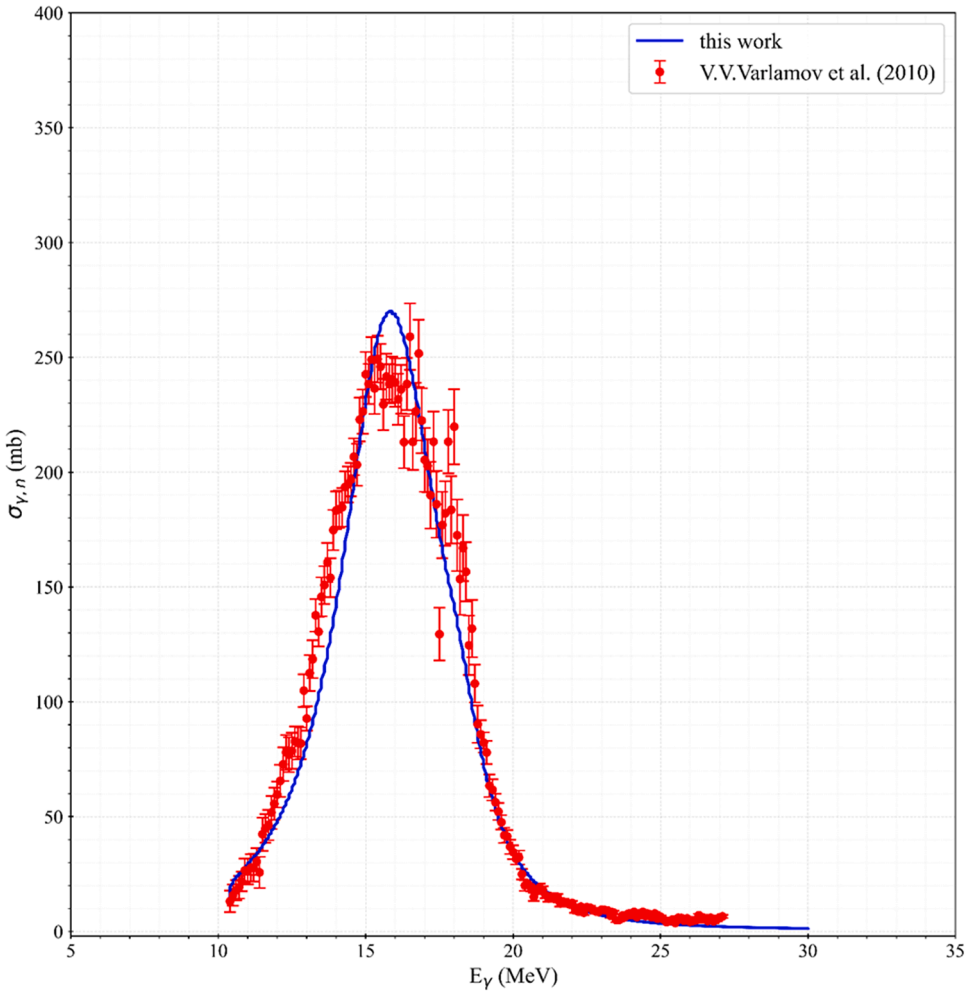

Fig. 9. Calculated (γ, n) reaction cross section for ^{114}Sn obtained within TALYS using neural-network-based GDR parameter systematics.

During training, Stage 2 and Stage 3 are conditioned on the experimental target values supplied by the dataset so that the width and peak-strength regressors learn their mappings with direct access to the relevant intermediate quantities. When applying the model to previously unobserved nuclides, those experimental values are not available; the pipeline is therefore executed sequentially by passing forward the preceding-stage predictions, i.e., Stage 2 uses $(X, E_{\mathrm{gdr,pred}})$ and Stage 3 uses $(X, E_{\mathrm{gdr,pred}}, \Gamma_{\mathrm{gdr,pred}})$.

To prevent information leakage arising from repeated records, the dataset is partitioned nucleus-wise rather than row-wise. The unique (Z, N, A) identifier is used as the splitting key, and all records for a given nuclide are assigned to the same subset. The same nucleus-wise partition is applied consistently across all three stages, ensuring that reported performance reflects extrapolation to nuclei absent from the training set.

The compiled dataset contains 117 total records corresponding to 86 unique nuclides. Under the nucleus-wise holdout protocol, 60 unique nuclides (69.8%) were assigned to the training subset, 13 (15.1%) to validation, and 13 (15.1%) to test. Since some nuclides are represented by multiple records, the corresponding record counts were 82 (70.1%), 17 (14.5%), and 18 (15.4%), respectively. These values are reported in order to make the statistical composition of the dataset and the effective strictness of the nucleus-wise split explicit. No nuclide was shared across subsets at any stage of the pipeline.

All stages used the same feed-forward multilayer perceptron architecture comprising three hidden layers of ten neurons each (Fig. 1). Training was performed with the Levenberg–Marquardt backpropagation algorithm [24,25], selected for its convergence behavior in moderate-scale regression problems. In the implemented script, the maximum number of epochs was explicitly set to 500. No custom early-stopping hyperparameter was manually introduced; therefore, the built-in stopping behavior associated with validation monitoring was retained. Architectural and training hyperparameters were held fixed across stages so that differences in performance reflect the staged construction rather than stage-specific retuning.

To complement the predictive analysis with an explicit interpretability layer, a SHAP (Shapley Additive Explanations)-based feature-importance analysis was performed separately for each stage of the sequential ANN framework. For Stage 1, SHAP values were evaluated for the eight base nuclide descriptors in X. For Stages 2 and 3, the analysis was carried out on the augmented input sets used by the corresponding regressors, namely $(X, E_{\mathrm{gdr,exp}})$ and $(X, E_{\mathrm{gdr,exp}}, \Gamma_{\mathrm{gdr,exp}})$, respectively, so that the relative contributions of both the original nuclide descriptors and the stage-conditioning variables could be examined within the same framework. Mean absolute SHAP values were normalized and expressed as relative percentage contributions in order to obtain stage-wise importance rankings. Since several nuclear descriptors are mutually correlated, particularly Z, N, A, and R, the SHAP results are interpreted here as model-based measures of relative influence within the trained ANN rather than as strictly independent causal effects. The resulting importance distributions are presented in Figs. 5–7.

Following training, the predicted parameter triplets were implemented in TALYS by overriding the default E1-strength parameterization. Implementation was carried out using the Brink–Axel Lorentzian [26,27] option (strength function type 2), which permits explicit

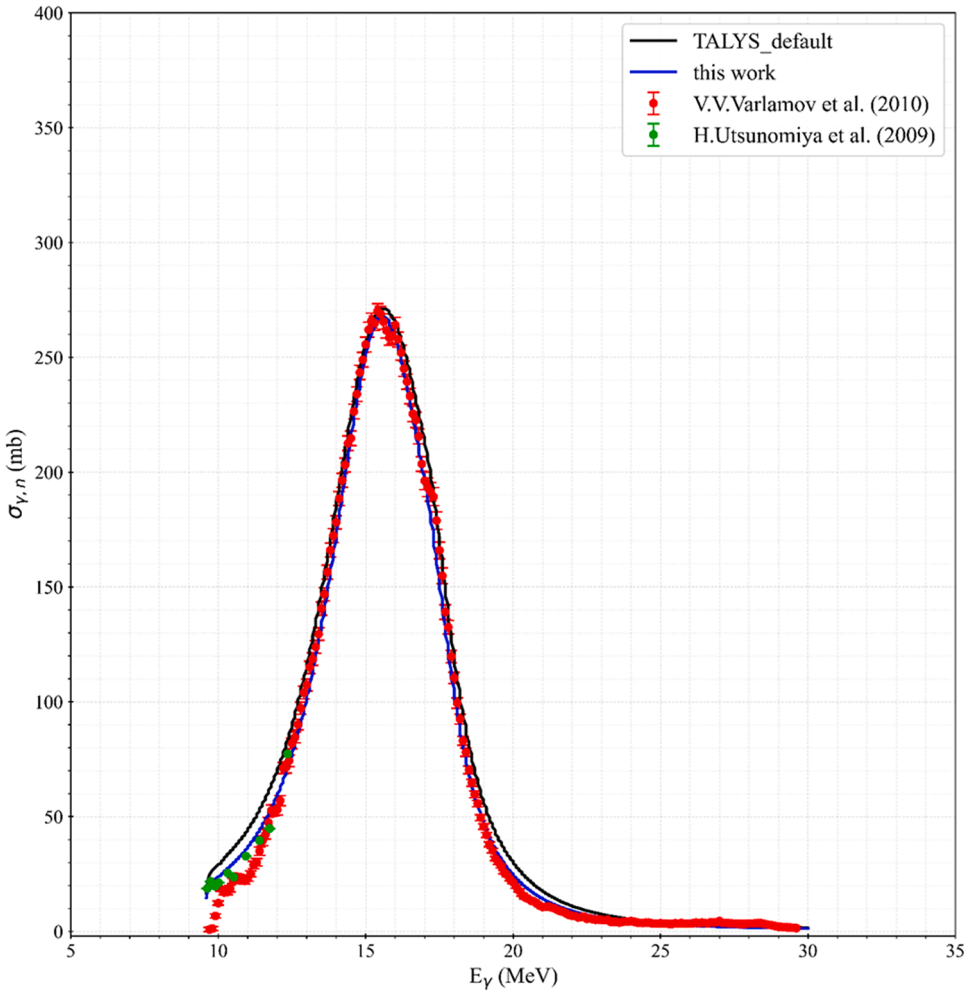

Fig. 10. Calculated (γ, n) reaction cross section for ^{116}Sn obtained within TALYS using neural-network-based GDR parameter systematics, compared with calculations based on the built-in GDR parameterization of TALYS.

specification and overriding of the GDR centroid energy, width, and peak cross section in the TALYS input. Calculations are performed under identical reaction-model settings using both ANN-derived GDR parameters and, when available, the built-in TALYS GDR entries, so that any differences in the resulting (γ,n) reaction excitation functions can be attributed solely to the adopted dipole parameters. Photoneutron reaction excitation functions are then calculated under identical reaction-model settings, allowing a controlled assessment of how the inferred GDR parameters propagate to observable (γ,n) reaction cross sections. Experimental excitation-function data used for validation were obtained from the EXFOR database [28] and accessed via the JANIS [29] nuclear data interface. Because the present ANN–TALYS workflow is deterministic, no statistically calibrated uncertainty band is reported for the calculated (γ,n) reaction cross sections.

$$E_{gdr,pred} = f_1(X) \tag{7}$$

$$\Gamma_{gdr,pred} = f_2(X, E_{gdr,exp}) \tag{8}$$

$$\sigma_{gdr,pred} = f_3(X, E_{gdr,exp}, \Gamma_{gdr,exp}) \tag{9}$$

3. Results

The predictive performance of the staged ANN framework is summarized in Figs. 2–4, which present regression results for training, validation, test, and combined datasets under nucleus-wise partitioning. Each figure corresponds to one of the three inferred GDR parameters within the sequential pipeline.

Fig. 2 reports the ANN estimations for E_{gdr}, the GDR centroid energy, with consistently high correlations across the subsets (Train$R \approx 0.999$, Validation$R \approx 0.993$, Test$R \approx 0.991$, All$R \approx 0.996$). Fig. 3 presents the corresponding results for Γ_{gdr}, the GDR width (Train$R \approx 0.993$, Validation$R \approx 0.963$, Test$R \approx 0.961$, All$R \approx 0.972$). Fig. 4 displays the regression for σ_{gdr}, the GDR peak cross section (Train $R \approx 0.98$, Validation $R \approx 0.963$, Test $R \approx 0.962$, All $R \approx 0.975$).

Taken together, Figs. 2–4 indicate that, for all three parameters, the validation and test correlations remain close to the training values, consistent with stable transfer to nuclides not included in the training subset. The close agreement between validation and test statistics supports the effectiveness of nucleus-wise partitioning in mitigating leakage from repeated records, since all entries associated with a given nuclide are confined to a single subset and the evaluation therefore probes nuclides genuinely held out from training. Accordingly, the reported regression performance is consistent with nuclide-level generalization rather than sensitivity to repeated measurements of the same nucleus that are often present in compiled photonuclear reaction datasets.

To examine how the trained ANN distributes importance among the input quantities, a SHAP-based relative-importance analysis was performed for each stage of the sequential framework, as shown in Figs. 5–7. The resulting importance patterns are clearly stage dependent and are consistent with the physical role assigned to each regressor in the staged construction. Rather than indicating an undifferentiated black-box dependence on the full input set, the analysis shows that the

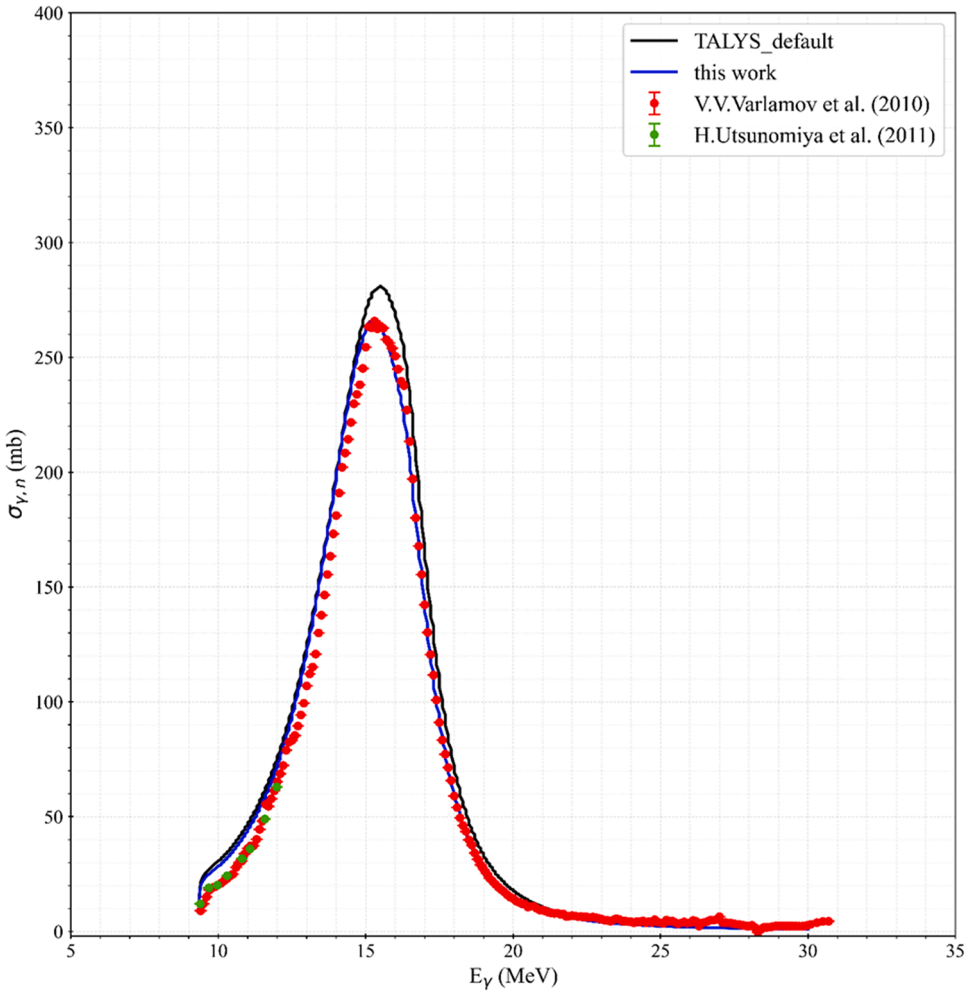

Fig. 11. Calculated (γ, n) reaction cross section for ^{118}Sn obtained within TALYS using neural-network-based GDR parameter systematics, compared with calculations based on the built-in GDR parameterization of TALYS.

network organizes the inference around a limited number of dominant descriptors at each stage.

As shown in Fig. 5, For Stage 1, corresponding to the inference of E_{gdr}, the largest relative contribution is associated with the asymmetry term $\frac{N-Z}{A}$, followed by N and R. Secondary contributions arise from β_2 and $\frac{BE}{A}$, whereas S_n, Z, and A play comparatively smaller roles within the trained model. This ranking is physically reasonable, since the centroid-energy systematics are expected to reflect global composition and size-related nuclear properties, together with a more limited sensitivity to deformation and binding-related structure effects.

As shown in Fig. 6, For Stage 2, corresponding to the inference of Γ_{gdr}, the asymmetry term again appears as the most influential quantity. The conditioned centroid-energy input $E_{\mathrm{gdr,exp}}$ also carries substantial relative importance, followed closely by $\frac{BE}{A}$ and R. The remaining descriptors contribute at lower, but still non-negligible, levels. This distribution is consistent with the staged formulation adopted here, in which the width regressor is expected to reflect not only bulk nuclear characteristics but also the resonance-energy scale inherited from the preceding stage.

As shown in Fig. 7, For Stage 3, corresponding to the inference of σ_{gdr}, the dominant contributions are associated with N and the conditioned centroid-energy input $E_{\mathrm{gdr,exp}}$, followed by Z, $\frac{BE}{A}$, and A. By comparison, R, $\Gamma_{\mathrm{gdr,exp}}$, S_n, $\frac{N-Z}{A}$, and β_2 make smaller relative contributions. Within the trained model, therefore, the peak cross section is governed primarily by nucleon-content variables together with the conditioned resonance-energy information, while deformation-related effects remain comparatively limited for the nuclei represented in the present dataset.

Taken together, the SHAP results provide a physically interpretable complement to the regression metrics by making explicit which quantities are most influential in each stage of the GDR-parameter inference. In this sense, the staged ANN framework is not only predictive but also structurally interpretable, with the learned hierarchy of importance remaining consistent with established trends in GDR systematics.

To assess the practical implications of the inferred GDR parameter systematics, a focused analysis was carried out along the even–even tin isotopic chain ($^{112-124}$Sn). Using the TALYS implementation and fixed-model protocol described in Methods, reaction excitation functions obtained with ANN-derived GDR parameters were compared with those from the built-in TALYS defaults (where available) and evaluated against selected EXFOR photoneutron reaction datasets accessed via JANIS.

Table 1 lists the centroid energy E, width Γ, and peak cross section σ for $^{112-124}$Sn, together with goodness of fit indicators (Red.χ^2, R^2, and pearson r) for the calculated (γ,n) reaction excitation functions relative to the selected EXFOR datasets [30–42]. For ^{112}Sn, ^{114}Sn, and ^{122}Sn, corresponding built-in GDR entries are absent in the TALYS 2.0 data file (Sn.gdr in structure/gamma/gdr/); accordingly, Table 1 reports only the ANN-derived parameter sets for these isotopes. In the absence of tabulated built-in entries, the staged ANN framework provides parameter triplets that follow smooth isotopic trends and enable TALYS calculations that remain compatible with the experimental reaction

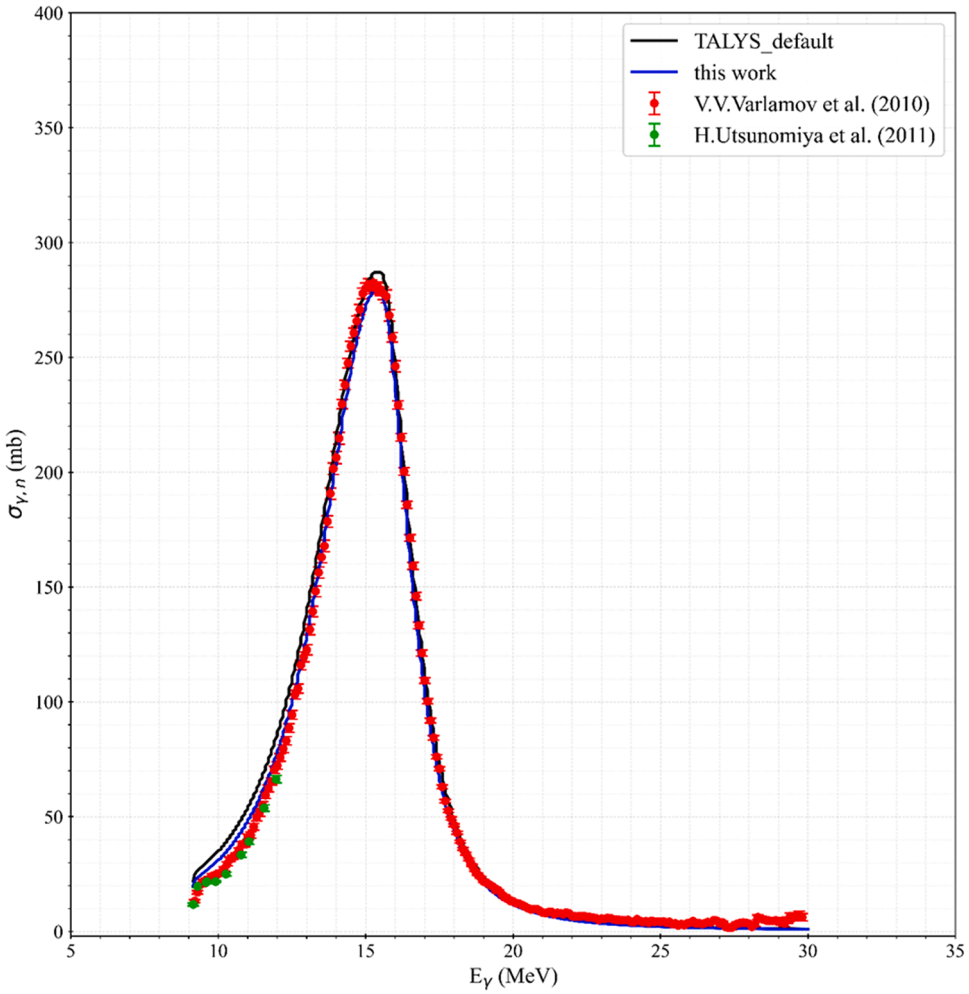

Fig. 12. Calculated (γ, n) reaction cross section for ^{120}Sn obtained within TALYS using neural-network-based GDR parameter systematics, compared with calculations based on the built-in GDR parameterization of TALYS.

excitation-function systematics under the same reaction-model settings.

Across the $^{112–124}$Sn sequence, the ANN-inferred centroid energies remain compatible with evaluated values where such entries exist. For isotopes ($^{116–120}$Sn and ^{124}Sn) with built-in parameters, differences between ANN-derived and tabulated values are systematic rather than erratic, preserving isotopic continuity. The ANN-derived widths are modestly lower than the built-in values for several nuclei, implying narrower dipole-strength distributions; this adjustment is reflected directly in the shape and peak region of the calculated photoneutron reaction excitation functions.

At the reaction level, as shown in Figs. 8–14, the ANN-based parameterization is consistently competitive with, and in several nuclei improves upon, the default parameter choice as assessed by reduced χ^2 and correlation measures. Notably, for ^{116}Sn,^{118}Sn, and ^{120}Sn, reduced χ^2 values decrease when ANN-derived parameters are used, while for ^{124}Sn the ANN-based results remain comparable to those obtained with the default evaluation. For ^{112}Sn, ^{114}Sn, and ^{122}Sn, where no corresponding built-in GDR entries are available in the TALYS 2.0 data file, calculations performed only with the ANN-derived parameter sets remain consistent with the experimental reaction excitation-function systematics under the same reaction-model settings. Across the chain, R^2 and Pearson r remain high, and no isotope shows a systematic loss of correlation when the ANN-based parameters are substituted. Overall, the substitution of the ANN-derived triplets mitigates isotope-dependent residual structures without compromising the global excitation-function trend.

In summary, the tin-isotope case study demonstrates that the staged ANN framework produces GDR parameter systematics that are internally coherent under nucleus-wise validation, can be integrated into TALYS through direct parameter override without altering other model ingredients, and yield stable reaction-level performance across a contiguous isotopic sequence. The approach therefore provides a practical alternative to heterogeneous or incomplete built-in parameter entries in photonuclear reaction modeling, particularly when isotopic continuity and controlled extrapolation are central requirements.

4. Conclusion

This work introduced and tested a staged artificial neural network framework to infer Lorentzian GDR parameters $\left(E_{\mathrm{gdr}}, \Gamma_{\mathrm{gdr}}, \sigma_{\mathrm{gdr}}\right)$ from a physically motivated set of eight nuclide descriptors $\left(Z, N, A, \frac{BE}{A}, S_n, R, \frac{N-Z}{A}, \beta_2\right)$. A central design choice was the use of nucleus-wise data partitioning, whereby all records associated with a given nuclide were assigned to a single subset. In compiled photonuclear reaction datasets that contain multiple entries per nucleus, this split provides a stringent evaluation setting and yields performance estimates that better reflect transfer to nuclei not represented during training. The regression results (Figs. 2–4) show that high correlations were maintained across training, validation, and test subsets for all three parameters, with validation–test consistency supporting genuine nuclide-level generalization under the

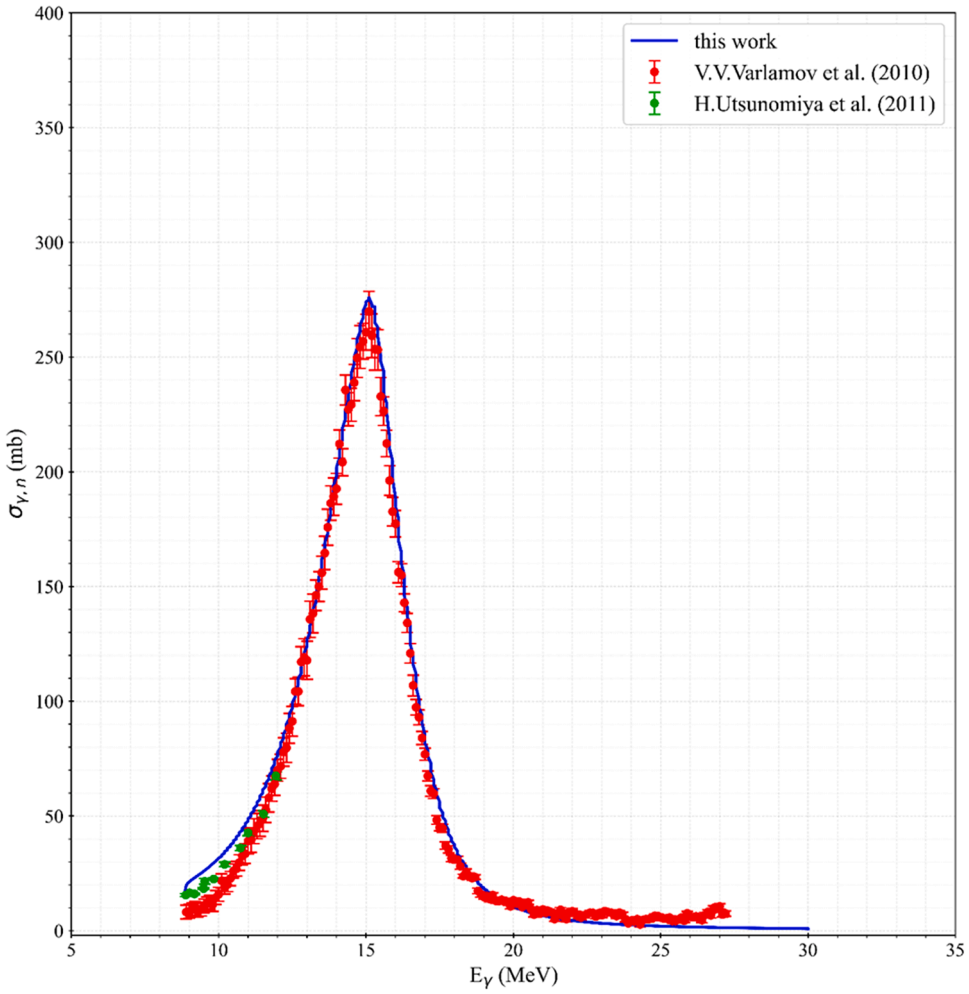

Fig. 13. Calculated (γ, n) reaction cross section for ^{122}Sn obtained within TALYS using neural-network-based GDR parameter systematics.

adopted splitting protocol. Overall, this workflow integrates evaluated nuclear-structure inputs (NNDC), evaluated GDR parameter systematics (RIPL-3), staged ANN inference, and reaction-model validation into a single internally consistent chain.

To assess the practical implications of the inferred systematics, the ANN-derived parameter triplets were implemented in TALYS 2.0 through direct override of the default E1-strength parameterization using the Brink–Axel Lorentzian option (strength function type 2), leaving all other reaction-model ingredients unchanged. Using the fixed-model calculation protocol described in Methods, the reaction-level impact was evaluated on the even–even $^{112–124}$Sn isotopic chain by comparing calculated (γ,n) reaction excitation functions with selected EXFOR photoneutron reaction datasets accessed via JANIS, and where available, against calculations obtained with the built-in TALYS GDR entries.

For isotopes ($^{116–120}$Sn and ^{124}Sn) with built-in TALYS entries, the ANN-based parameterization was generally competitive with the default choice and, in several cases, yielded lower reduced χ^2 values (notably for ^{116}Sn, ^{118}Sn, and ^{120}Sn) while remaining comparable for ^{124}Sn, with high R^2 and Pearson r maintained throughout. For ^{112}Sn, ^{114}Sn, and ^{122}Sn, where no corresponding built-in GDR entries were available in the TALYS 2.0 data file, the ANN-derived parameter sets provided a consistent basis for TALYS calculations and produced (γ,n) reaction excitation functions that were compatible with the experimental systematics under the same modeling conditions. Collectively, these results indicate that the staged construction delivers internally coherent GDR parameter trends that propagate in a controlled manner to observable photoneutron reaction cross sections along a contiguous isotopic sequence.

Beyond the tin-chain demonstration, the study highlights two methodological points that are broadly relevant for data-driven photonuclear reaction modeling. First, nucleus-wise partitioning can be regarded as the default validation protocol when datasets contain repeated records per nuclide and when the scientific objective concerns systematic behavior across nuclei. Second, staged conditioning offers a transparent means of reflecting the known interdependence among GDR parameters within the learning task without imposing a fixed analytic coupling, while retaining the full descriptor information at each stage. A further SHAP-based interpretability analysis showed that the trained regressors exhibit distinct and physically meaningful stage-dependent importance patterns. In the centroid-energy stage, the dominant contributions arise from asymmetry, neutron content, and radius-related information. In the width stage, asymmetry, the conditioned centroid-energy input, $\frac{BE}{A}$, and A were the leading quantities. In the peak-cross-section stage, the inference is governed primarily by neutron and proton content together with the conditioned resonance parameters. These results add an explicit interpretability layer to the ANN framework and support its use as a physically informed parameterization strategy rather than a purely opaque regression scheme. Within this scope, the staged ANN framework provides a practical and internally consistent complement to heterogeneous or incomplete built-in parameter entries, particularly in applications where isotopic continuity and controlled extrapolation across nuclides are central requirements.

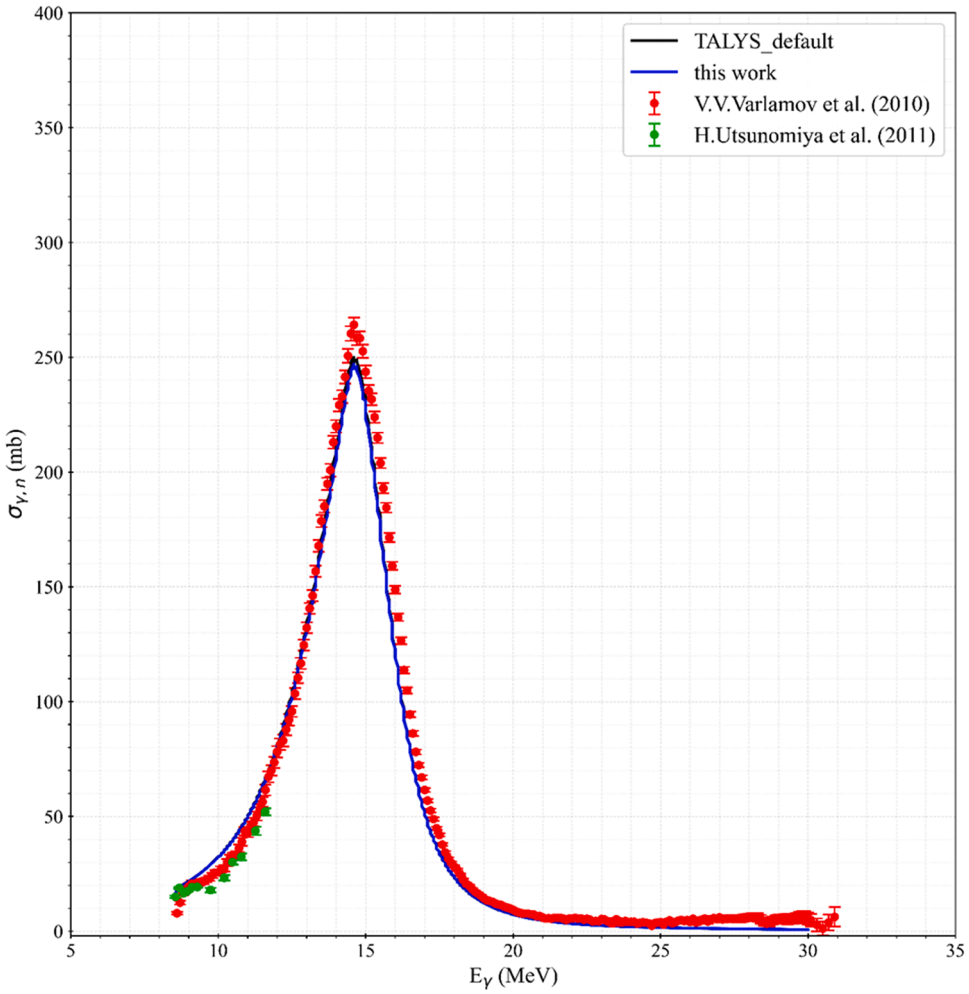

Fig. 14. Calculated (γ, n) reaction cross section for ^{124}Sn obtained within TALYS using neural-network-based GDR parameter systematics, compared with calculations based on the built-in GDR parameterization of TALYS.

CRediT authorship contribution statement

Murat Dag: Writing – review & editing, Writing – original draft, Visualization, Validation, Supervision, Software, Methodology, Investigation, Formal analysis, Data curation, Conceptualization.

Declaration of competing interest

The authors declare that they have no known competing financial interests or personal relationships that could have appeared to influence the work reported in this paper.

Data availability

The data that has been used is confidential.

References

[1] R.B. Firestone, "The Origin of the Giant Dipole Resonance,", arXiv:2009.03356 [nucl-th] (2021) rev.
[2] IAEA, "Handbook on photonuclear data for applications cross-sections and spectra", vol. 7, p. 284, 2000.
[3] H. Steinwedel, J.H.D. Jensen, P. Jensen, Nuclear dipole vibrations, Phys. Rev. 79 (6) (1950) 1019, https://doi.org/10.1103/PhysRev.79.1019. Sep.
[4] M. Goldhaber, E. Teller, On nuclear dipole vibrations, Phys. Rev. 74 (9) (1948) 1046–1049, https://doi.org/10.1103/PhysRev.74.1046.
[5] G.F. Bertsch, P.F. Bortignon, R.A. Broglia, Damping of nuclear excitations, Rev. Mod. Phys. 55 (1) (1983) 287, https://doi.org/10.1103/RevModPhys.55.287. Jan.
[6] J. Speth, A. Van Der Woude, Giant resonances in nuclei, Rep. Prog. Phys. 44 (7) (1981) 719, https://doi.org/10.1088/0034-4885/44/7/002. Jul.
[7] J.S. Levinger, H.A. Bethe, Dipole transitions in the nuclear photo-effect, Phys. Rev. 78 (2) (1950) 115, https://doi.org/10.1103/PhysRev.78.115. Apr.
[8] G.I. Opat, The electric dipole sum rule, Nucl. Phys. 14 (3) (1960) 506–511, https://doi.org/10.1016/0029-5582(60)90468-5. Jan.
[9] T. Kawano, et al., IAEA photonuclear data library 2019, Nucl. Data Sheets 163 (2020) 109–162, https://doi.org/10.1016/j.nds.2019.12.002.
[10] E.G. Fuller, M.S. Weiss, Splitting of the giant resonance for deformed nuclei, Phys. Rev. 112 (2) (1958) 560–567, https://doi.org/10.1103/PhysRev.112.560.
[11] B.L. Berman, S.C. Fultz, Measurements of the giant dipole resonance with monoenergetic photons, Rev. Mod. Phys. 47 (3) (1975) 713–761, https://doi.org/10.1103/RevModPhys.47.713.
[12] S.S. Wang, Y.G. Ma, X.G. Cao, W.B. He, H.Y. Kong, C.W. Ma, Investigation of giant dipole resonances in heavy deformed nuclei with an extended quantum molecular dynamics model, Phys. Rev. C 95 (5) (2017) 1–7, https://doi.org/10.1103/PhysRevC.95.054615.
[13] T. Mukhopadhyay, D.N. Basu, Photonuclear reactions of actinides in the giant dipole resonance region, Eur. Phys. J. A 45 (1) (2010) 121–124, https://doi.org/10.1140/epja/i2010-10993-y.
[14] R. Weiss, B. Bazak, N. Barnea, The generalized nuclear contact and its application to the photoabsorption cross-section, Eur. Phys. J. A 52 (4) (2016) 1–6, https://doi.org/10.1140/epja/i2016-16092-3.
[15] R. Capote, et al., RIPL – reference input parameter library for calculation of nuclear reactions and nuclear data evaluations, Nucl. Data Sheets 110 (12) (2009) 3107–3214, https://doi.org/10.1016/J.NDS.2009.10.004. Dec.
[16] "RIPL-3: reference input parameter library". Accessed: Feb. 23, 2026. [Online]. Available: https://www-nds.iaea.org/RIPL-3.
[17] M. Kumar Bairwa and P. Arumugam, "Machine learning approaches for giant dipole resonance parameters", 2020.
[18] Y.A. Üncü, et al., Calculations of GDR parameters for deformed nuclei using LogitBoost classifier and artificial neural network, MPLA 37 (13) (2022), https://doi.org/10.1142/S0217732322500791, 2250079–22Apr.

[19] J.H. Bai, Z.M. Niu, B.Y. Sun, Y.F. Niu, The description of giant dipole resonance key parameters with multitask neural networks, Phys. Lett. Sect. B Nucl. Elem. Part. High-Energy Phys. 815 (2021), https://doi.org/10.1016/j.physletb.2021.136147. Feb.
[20] X. Wang, L. Zhu, J. Su, Providing physics guidance in bayesian neural networks from the input layer: the case of giant dipole resonance predictions, Phys. Rev. C 104 (3) (2021) 034317, https://doi.org/10.1103/PhysRevC.104.034317. Sep.
[21] H. Özdoğan, Y. Ali Üncü, O. Karaman, M. Şekerci, A. Kaplan, Estimations of giant dipole resonance parameters using artificial neural network, Appl. Radiat. Isot. 169 (2020) 2021, https://doi.org/10.1016/j.apradiso.2020.109581. October.
[22] K. A, H. S, and G. S, "TALYS-1.96/2.0 simulation of nuclear reactions", 2021.
[23] NNDC, Accessed: Feb. 23, https://www.nndc.bnl.gov/nudat3, 2026.
[24] K. Levenberg, a method for the solution of certain non-linear, Q. Appl. Math. 2 (2) (1944) 4164–4168.
[25] D.W. Marquardt, Alternatieve klinisch-chemische laboratoria: leveranciers van onjuiste of niet-bestaande diagnosen, Ned. Tijdschr. Geneeskd. 151 (51) (1963) 2816–2819.
[26] D.M. Brink, Individual particle and collective aspects of the nuclear photoeffect, Nucl. Phys. 4 (1957) 215–220, https://doi.org/10.1016/0029-5582(87)90021-6, no. CAug.
[27] P. Axel, Electric dipole ground-State transition width strength function and 7-mev photon interactions, Phys. Rev. 126 (2) (1962) 671, https://doi.org/10.1103/PhysRev.126.671. Apr.
[28] V.V. Zerkin, B. Pritychenko, The experimental nuclear reaction data (EXFOR): extended computer database and web retrieval system, Nucl. Instruments Methods Phys. Res. Sect. A Accel. Spectrometers, Detect. Assoc. Equip. 888 (2018) 31–43, https://doi.org/10.1016/j.nima.2018.01.045. Apr.
[29] JANIS, Accessed: Feb. 23, https://www.oecd-nea.org/janisweb, 2026.
[30] V.V. Varlamov, B.S. Ishkhanov, V.N. Orlin, V.A. Chetvertkova, Evaluated cross sections of the σ(γ, nX) and σ(γ, 2nX) reactions on 112, 114, 116, 117, 118, 119, 120, 122, 124Sn isotopes, Bull. Russ. Acad. Sci. Phys. 74 (6) (2010) 833–841, https://doi.org/10.3103/S1062873810060225, 2010 746volJul.
[31] B.S. Ishkhanov, S.Y. Troshchiev, V.A. Chetvertkova, Yields of photonuclear reactions on Sn isotopes at an energy of 29.1 MeV, Bull. Russ. Acad. Sci. Phys. 76 (4) (2012) 481–485, https://doi.org/10.3103/S1062873812040168, 2012 764volMay.
[32] V.V. Varlamov, B.S. Ishkhanov, V.N. Orlin, N.N. Peskov, K.A. Stopani, Photoneutron reactions in astrophysics, Phys. At. Nucl. 77 (12) (2014) 1491–1504, https://doi.org/10.1134/S1063778814110088, 2014 7712Dec.
[33] S.C. Fultz, B.L. Berman, J.T. Caldwell, R.L. Bramblett, M.A. Kelly, Photoneutron cross sections for Sn116, Sn117, Sn118, Sn119, Sn120, Sn124, and indium, Phys. Rev. 186 (4) (1969) 1255–1270, https://doi.org/10.1103/PhysRev.186.1255. Oct.
[34] H. Utsunomiya, et al., ray strength function for 116,117 Sn with the pygmy dipole resonance balanced in the photoneutron and neutron capture channels, Phys. Rev. C 80 (5) (2009) 055806, https://doi.org/10.1103/PhysRevC.80.055806. Nov.
[35] M. Kamata, et al., Extra γ-ray strength for 116,117Sn arising from pygmy dipole resonance, AIP Conf. Proc. 1238 (1) (2010) 234–236, https://doi.org/10.1063/1.3455938. Jun.
[36] H. Utsunomiya, et al., The γ-ray strength function in nuclear astrophysics, AIP Conf. Proc. 1120 (1) (2009) 183–188, https://doi.org/10.1063/1.3141644. May.
[37] B.S. Ishkhanov, V.N. Orlin, V.V. Varlamov, Total and partial photoneutron reactions cross sections – new analysis and evaluation, EPJ Web Conf 38 (2012) 12003, https://doi.org/10.1051/epjconf/20123812003.
[38] Д. А. И. V.V. Varlamov, B.B.B.A.I. Davydov, V.N. Orlin, Partial photoneutron reaction cross sections in experiments with bremsstrahlung Bull. Russ. Acad. Sci. Phys. 87 (8) (2023) 1176–1185, https://doi.org/10.31857/s0367676523702113. Aug
[39] H. Utsunomiya, et al., Photoneutron cross sections for 118–124Sn and the ?-ray strength function method, Phys. Rev. C 84 (5) (2011) 055805, https://doi.org/10.1103/PhysRevC.84.055805. Nov.
[40] V.V. Varlamov, A.I. Davydov, V.N. Orlin, Photodisintegration of 127 I: systematic uncertainties of experiments and data evaluated using physical criteria, Am. J. Phys. Appl. 8 (5) (2020) 64–72, https://doi.org/10.11648/j.ajpa.20200805.11.
[41] A.V. Chekhovska, I.L. Semisalov, V.I. Kasilov, Y.O. Skakun, Stellar nucleosynthesis: experimental yields of the 112Sn(γ,n)111Sn and 112Sn(γ,p)111m,gIn reactions for p-nuclei production simulation, Springer Proc. Phys. 219 (2019) 301–305, https://doi.org/10.1007/978-3-030-13876-9_52.
[42] C. Kuo, B.S. Ratner, B.V. Sergeev, An investigation of the 112Sn(γ,n) and 124Sn(γ, n) reactions, Zhur. Eksptl'. i Teoret. Fiz. 40 (1) (1961) 85–87.